Electrochemistry Communications 115 (2020) 106713

Contents lists available at ScienceDirect

Electrochemistry Communications

journal homepage: www.elsevier.com/locate/elecom

High-performance ion removal via zinc–air desalination

Pattarachai Srimuk[a], Lei Wang[a,b], Öznil Budak[a,b], Volker Presser[a,b,*]

[a] INM – Leibniz Institute for New Materials, 66123 Saarbrücken, Germany
[b] Department of Materials Science and Engineering, Saarland University, 66123 Saarbrücken, Germany

ARTICLE INFO

Keywords:
Water desalination
Capacitive deionization
Zinc-air battery
Oxygen reduction reaction
Oxygen evolution reaction

ABSTRACT

Electrochemical processes enable a new generation of energy-efficient desalination technologies. While ion electrosorption via capacitive deionization is only suitable for brackish water with low molar strength, the use of Faradaic materials capable of reversible ion intercalation or conversion reactions allows energy-efficient removal of ions from seawater. However, the limited charge transfer/storage capacity of Faradaic materials indicates an upper limit for their desalination applications. Therefore, a new electrochemical concept must be explored to exceed the current state-of-the-art results and to push the desalination capacity beyond 100–200 $mg_{NaCl}/g_{electrode}$. In this proof-of-concept work, we introduce the new concept of using metal–air battery technology for desalination. We do so by presenting performance data for zinc–air desalination (ZAD) in 600 mM NaCl. The ZAD cell provides a desalination capacity of 0.9–1.0 mg_{NaCl}/cm^2 (normalized to the membrane area; corresponding to 1300 mg_{NaCl}/g_{Zn}) with a charge efficiency of 70% when charging/discharging the cell at 1 mA/cm^2. The energy consumption of ZAD is 68–92 kJ/mol.

1. Introduction

Energy and water are two fundamental resources for our technological society and industry. With growing environmental awareness and continued consumption of resources alongside increased pollution, there is a tremendous need for low-energy, high-performance technologies capable of producing fresh water, as alternatives to such methods as reverse osmosis [1]. In contrast to pressure or filtration-based desalination and ion separation technologies, there is great promise in electrochemical processes. In addition to the feature of ion separation (accomplished with invested charge), electrochemical processes also offer the dual-use benefit of intermittent energy storage, because most of the invested charge is recovered during electrode regeneration [2]. Capacitive deionization (*first-generation electrochemical desalination*) achieves energy-efficient salt removal by ion electrosorption with nanoporous carbon electrodes; however, this mechanism limits effective remediation to brackish water (< 100 mM NaCl) with a desalination capacity of about 20–30 $mg_{NaCl}/g_{electrode}$ [3,4]. Faradaic deionization (FDI, or *second-generation electrochemical desalination*), in contrast, allows effective desalination also at higher molar strengths. The desalination capacity has been reported to approach 200 $mg_{NaCl}/g_{electrode}$ for intercalation materials (e.g., $Na_{0.44}MnO_2$, NASICON-type $NaTi_2(PO_4)_3$, MXene) [5–8], redox electrolytes (e.g., iodide or bromide based) [9,10], or conversion materials (e.g., BiOCl, Ag/AgCl) [11,12]. However, to achieve even higher desalination capacities, it is necessary to capitalize on electrochemical processes and materials that offer a much higher charge storage capacity than 200–300 mAh/g since salt removal directly correlates with this property [12].

The search for a *third-generation electrochemical desalination* technology has inspired us to adopt, for the first time, the concept used for high charge storage in metal–air batteries. As an example of the promising use of metal–air battery technology for desalination, we introduce zinc–air desalination (ZAD). The equipment consists of a Zn anode, an anion exchange membrane, a cation exchange membrane, and the air electrode. Instead of a rare and expensive catalyst material (e.g., Pt, RuO_2), we used MoS_2 as a catalyst for the cathode in ZAD. The resulting desalination performance is far superior to any CDI or FDI reported so far, and opens the way for a new class of electrochemical desalination.

2. Experimental

2.1. Material synthesis and characterization

MoS_2 (20 μm, Sigma Aldrich) was exfoliated using tip-sonication. Briefly, 10 mg of MoS_2 and 50 mg of NaOH (98%, Sigma Aldrich) were mixed with 200 mL N-methyl-2-pyrrolidone (NMP, Sigma Aldrich). The solid–liquid mixture was then subjected to sonication for 7.5 h with an

* Corresponding author at: INM – Leibniz Institute for New Materials, 66123 Saarbrücken, Germany.
E-mail address: volker.presser@leibniz-inm.de (V. Presser).

https://doi.org/10.1016/j.elecom.2020.106713
Received 28 February 2020; Received in revised form 16 March 2020; Accepted 18 March 2020
Available online 21 March 2020

output power of 200 W and a frequency of 40 kHz. During the sonication process, the suspension was kept in an ice-bath to compensate for the heat generated by the high-frequency vibration of the sonication process. After sonication, the resulting solution was centrifuged at 4000 rpm for 30 min. The supernatant was collected and then vacuum filtered through a polymer membrane (0.1 μm, Merck Millipore). After washing the filtrate several times with ethanol and water, the resulting powder was dried in a vacuum oven for 24 h and is termed "exfoliated MoS_2".

X-ray diffraction (XRD) was conducted with a D8 Discover diffractometer (Bruker AXS) with a copper source (Cu-K_α, 40 kV, 40 mA), a Göbel mirror, and a 1 mm point focus. A two-dimensional VANTEC-500 detector covered an angular range of 20° 2θ with frames recorded at 20°, 40°, and 80° 2θ using a measurement time of 1000 s per frame.

2.2. Electrochemical characterization

Two of the key factors in evaluating the performance of ZAD are the oxygen reduction reaction (ORR) and oxygen evolution reaction (OER). To do this, we conducted OER and ORR using a rotating-disk glassy carbon electrode (RDE). The RDE electrode was modified by drop-casting a catalyst slurry consisting of 80 mass% of catalyst materials, 10 mass% of carbon black (C65, Imerys Graphite& Carbon), 10 mass% of polyvinylidene fluoride (PVDF, Alfa Aesar), with NMP as the solvent. For comparison, we used RuO_2 (>99.9%, ThermoFisher) as the control standard catalyst. Before the experiment, 0.1 M NaOH was purged with O_2 for 20 min. A Pt coil and Ag/AgCl were used as the counter and reference electrode, respectively. To study the ORR, linear sweep voltammetry (LSV) was applied using a scan rate of 50 mV/s and a cut-off potential between −0.6 V and 0 V vs. Ag/AgCl. The Koutechy-Levich (K-L) equation was used to estimate the number of electrons transferred during ORR [13]. LSV was also applied to study the OER, using a sweep rate of 50 mV/s and a cut-off potential between 0.1 V and 1.6 V vs. Ag/AgCl.

2.3. Desalination performance

The ZAD cell consists of a Zn disk (Ø = 2.6 cm, 0.125 mm in thickness, 99.95% purity, GoodFellow), an anion exchange membrane (AEM, Ø = 3 cm, FAS-PET-130, Fumatech), a separator, a cation exchange membrane (CEM, Ø = 3 cm, FKS-PET-130, Fumatech), and a cathode catalyst (Ø = 2.6 cm). For the cathode and gas diffusion layer, we used a free-standing electrode fabricated from exfoliated MoS_2 and 10 mass% carbon nanotubes (CNTs, Nanocyl NC7000), similarly to our previous work on FDI [14]. The cell components were carefully placed in a multi-channel capacitive deionization (MCDI) cell. 1 M $ZnCl_2$ was confined between the Zn disk and the AEM, then 0.1 M NaOH was confined between the cathode and the CEM. The solution to be desalinated, 600 mM NaCl, was continuously fed (15 mL/min) into the middle channel of the cell. During operation, humid oxygen gas was continuously blown into the cathode side to supply enough O_2 for ORR during discharging. Chronopotentiometry with a current of 1 mA/cm^2 and a cut-cell voltage of 0–3 V was applied to charge and discharge the ZAD. Each charge and discharge step lasted 30 min. We followed our previous work [15] in the calculations of desalination capacity, charge capacity, and charge efficiency.

3. Results and discussion

3.1. Structural characterization

XRD patterns of the bulk and exfoliated MoS_2 are shown in Fig. 1, where the pattern of bulk MoS_2 is assigned to the 2H (hexagonal) phase of MoS_2 (PDF: 77-1716). The shifting of the (0 0 2) plane reflection is due to the exfoliation process. We also show the chosen focus area between 12° and 17° 2θ in Fig. 1 (inset). While bulk MoS_2 displays the (0 0 2) plane reflection at 14.5° 2θ, the corresponding reflection of exfoliated MoS_2 can be seen at 14.4 °2θ, with a lower intensity compared to that of the bulk MoS_2.

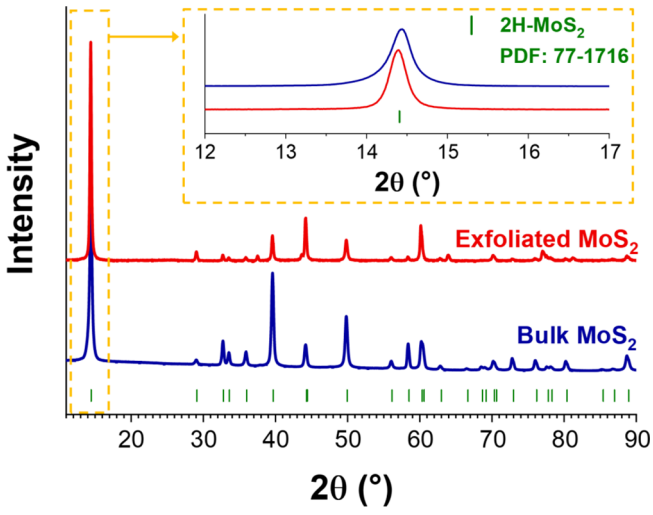

Fig. 1. X-ray diffractogram of bulk MoS_2 and exfoliated MoS_2.

3.2. Electrochemical characterization

The properties of the exfoliated MoS_2 as an electrochemical catalyst were compared with those of bulk MoS_2 and commercially available RuO_2. Fig. 2A shows the ORR activity of the modified RDE electrode. The half-wave potentials for exfoliated MoS_2 and bulk MoS_2 were observed to be higher than that of RuO_2, suggesting that MoS_2 exhibits better ORR catalytic activity. The ORR Tafel plot (Fig. 2B) clearly shows the effect of the exfoliation process on the charge transfer abilities of MoS_2, in that the exfoliated MoS_2 exhibits the fastest charge transfer. At different rotation rates of the modified RDE electrode, the diffusion-limited current increases, indicating the shortening of the O_2 diffusion path. The K-L (Koutecky-Levich) plots in Fig. 2C show that the reaction follows first-order kinetics via the concentration of dissolved oxygen. Thus, exfoliated MoS_2 shows a 4-electron transfer pathway for the ORR while the electron transfer figures for bulk MoS_2 and RuO_2 are 2.5 and 2.9, respectively (Fig. 2D).

The OER activity is shown in Fig. 2E-F. RuO_2 is known to be one of the best OER catalysts and has an onset potential of 0.45 V vs. Ag/AgCl while exfoliated MoS_2 and bulk MoS_2 exhibit onset potentials of ca. 0.5 V and 0.8 V vs. Ag/AgCl. The OER kinetics in exfoliated MoS_2 are faster at low overpotentials, resulting in a lower potential at the specific current of 10 mA/cm^2. Exfoliated MoS_2 has a lower Tafel slope than bulk MoS_2 (Fig. 2F). Based on the electrochemical performances, we can see that exfoliated MoS_2 is suitable for the cathode in ZAD as it is much cheaper than RuO_2 or a noble catalyst such as Pt. It can be estimated that, using an exfoliated MoS_2 cathode in ZAD, the maximum cell voltage is up to 1.6 V, depending on the charging and discharging current.

To test the electrochemical performance of exfoliated MoS_2, we assembled a zinc–air battery (ZAB; Fig. 3A). At a very low charge/discharge specific current of 0.1 mA/cm^2 (normalized by the membrane area), ZAB shows a cell voltage of 1.3 V with a specific capacity of 800 mAh/g_{Zn} (Fig. 3B) and an areal capacity of 0.8 mAh/cm^2. To demonstrate its cyclic stability, the ZAB was charged and discharged at 1 mA/cm^2 with a limited charge/discharge-time of 10 min. Over the course of

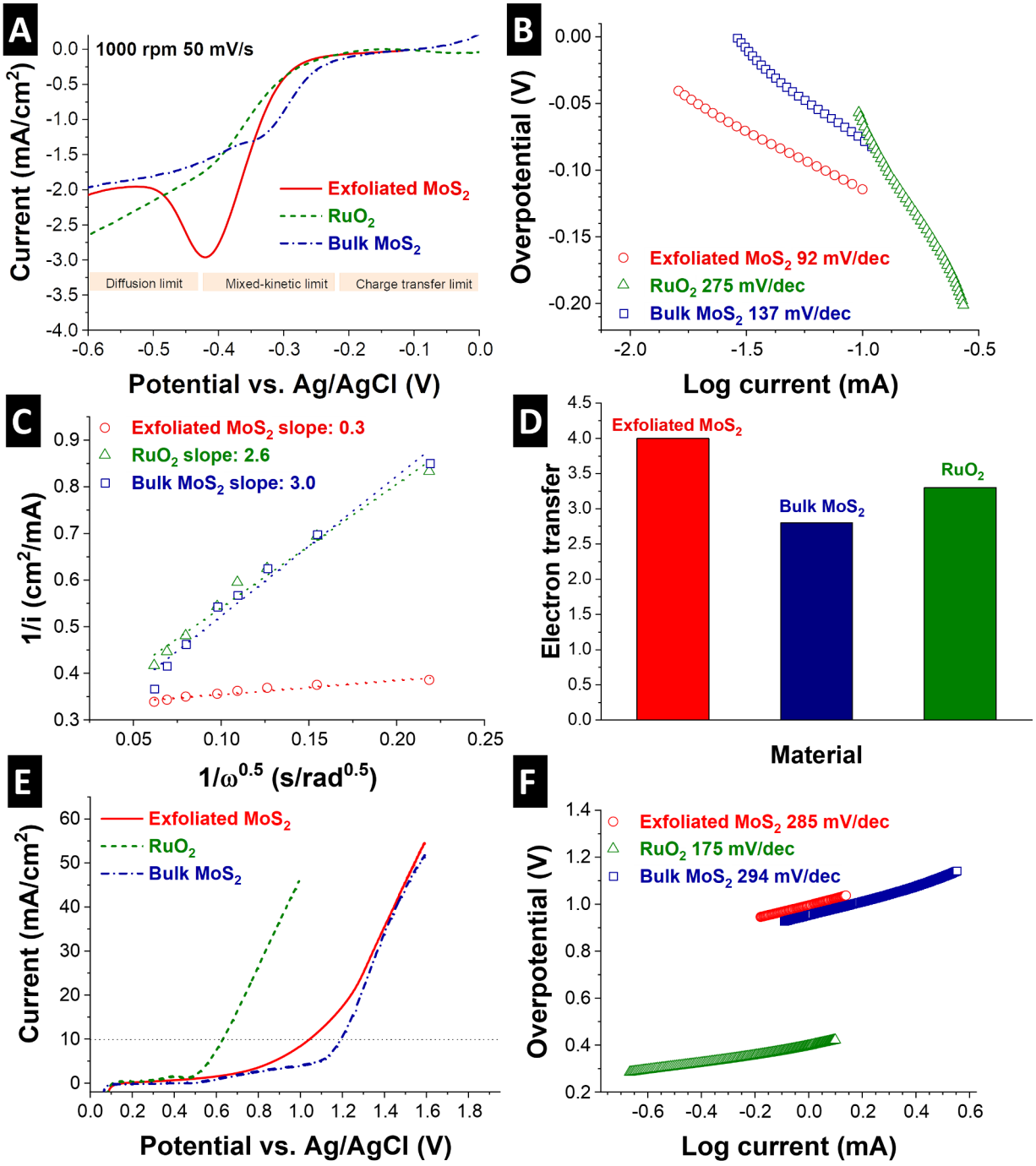

Fig. 2. Catalytic performance of exfoliated MoS_2, bulk MoS_2, and RuO_2: (A) ORR polarization curve; (B) ORR Tafel plot; (C) K-L plot; (D) the number of electrons transferred during ORR; (E) OER; and (F) OER Tafel plot. All experiments were conducted in O_2-saturated, aqueous 0.1 M NaOH.

25 cycles, the cell voltage is stable at 2.2 V, while the first cycle displays a cell voltage of 0.8 V (Fig. 3C). The specific capacity can be maintained at 150 mAh/g_{Zn} for 25 cycles (Fig. 3D). It is likely that ZnO formation on the side of the anode causes the increase in the cell voltage [16].

3.3. Desalination performance

After the desalination cell had been assembled (Fig. 4A), the desalination performance was tested using a feed salt concentration of 600 mM NaCl. At a current density of 1 mA/cm^2, the ZAD cell exhibits inverted desalination: ions are released during charging and desalination during discharging (Fig. 4B). As the cell is charged, the cell voltage is slowly increased due to the production of oxygen gas at the cathode while Zn^{2+} is deposited at the anode (Fig. 4A). As a result, Na^+ and Cl^- are ejected across the CEM and AEM, respectively. During discharge, the MoS_2 cathode undergoes ORR with a 4-electron transfer producing OH^- while anode Zn is stripped out. Consequently, Na^+ and Cl^- from the feed stream are removed (desalination). The charge/discharge capacity of ZAD is about 880 mAh/g_{Zn} (Fig. 4C), and this value corresponds to an areal capacity of 0.65 mAh/cm^2. For 20 cycles, the ZAD

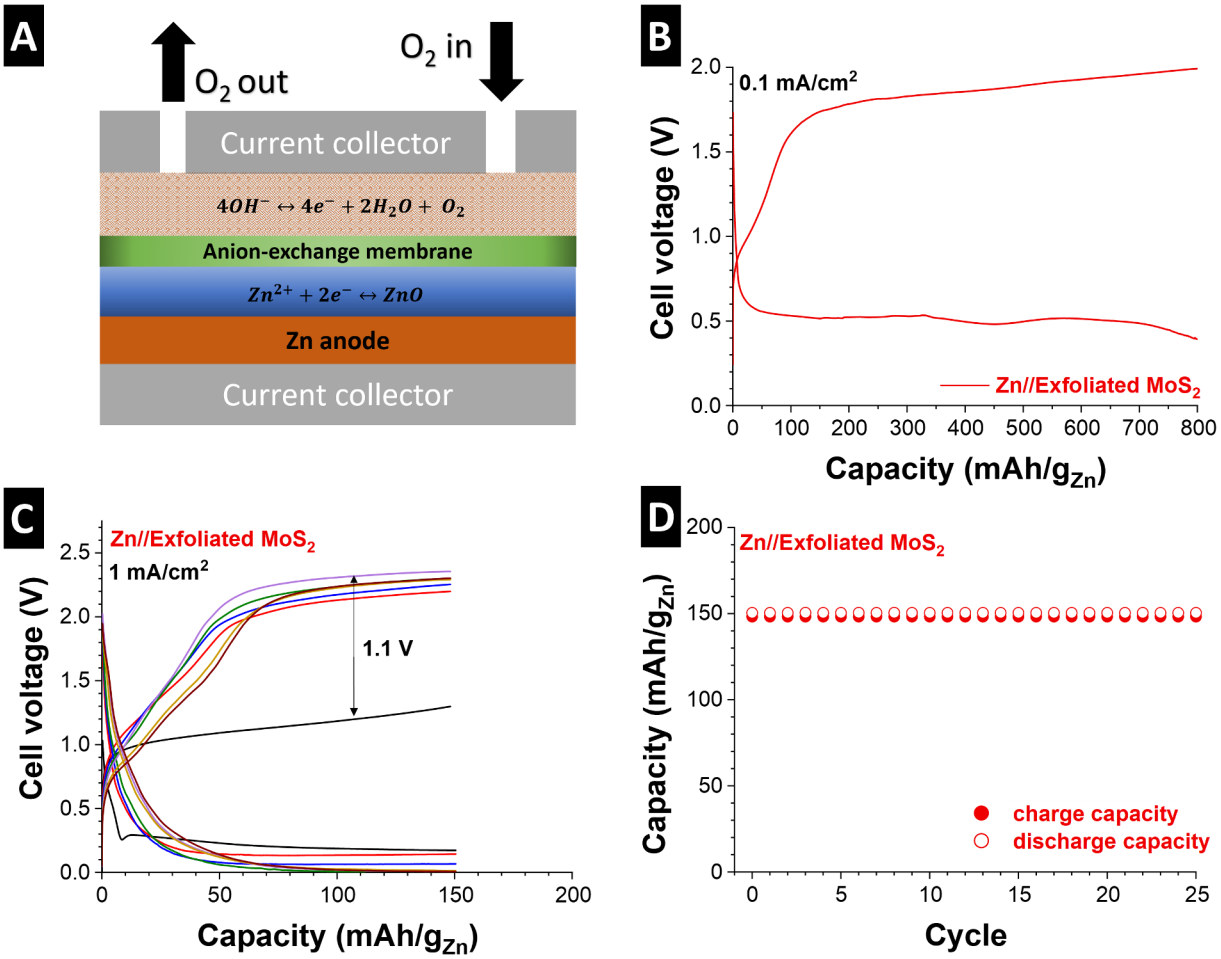

Fig. 3. Zinc–air battery performance: (A) illustration of ZAB cell configuration; (B) charge capacity of the ZAB cell at an areal current of 0.1 mA/cm^2; (C) cell voltage–capacity plot at an areal current of 1 mA/cm^2; (D) cyclic stability of ZAB.

cell provides a very high desalination capacity of 0.9–1.0 mg_{NaCl}/cm^2 (corresponding to a gravimetric desalination capacity of 1300 mg/g_{Zn}) with a charge efficiency of 70% (Fig. 4E). The ZAD performance normalized to the area of the ion-exchange membrane is remarkably high compared to membrane-enhanced CDI (MCDI; ca. 0.1 mg_{NaCl}/cm^2) or Ag/AgCl conversion-type FDI (ca. 0.2 mg_{NaCl}/cm^2), as shown in Fig. 4D [12,17]. To lower the ion concentration from 600 mM to 5 mM in a volume of 1 L in a single-pass, one-cycle operation, our ZAD unit would require an equivalent mass of 27 g of Zn; for comparison, one would need about 1.7 kg of nanoporous carbon (assuming a desalination capacity of 20 mg_{NaCl}/g_{carbon}) for a typical CDI cell.

The ZAD cell delivers a discharge of 2.2 mWh (564 Wh/kg_{Zn}) with a round-trip energy efficiency of ca. 30%. These values correspond to an energy consumption of 25–35 kT (Fig. 4F), which is equal to 68–92 kJ/mol. With a salt reduction of 0.03%, the energy per processed water is 0.008 Wh/L. 0.03% may seem a small value; however, the cell we used to process the saline medium was small, and we refer here to single-pass values for one cycle. As seen in Table 1, the energy consumption of ZAD is relatively low compared to a previous study using ion-insertion Faradaic materials, redox electrolyte, conversion material, and membrane CDI (0.2 Wh/L) [18].

In addition to MoS_2 (this work), the selection and design of cathode materials (e.g., metal oxides, layered metal hydroxides, and heteroatom doped carbon) [19] can potentially have a positive impact on battery performance as well as desalination performance. For example, by growing WS_2 directly onto CNTs, the interconnected interface between WS_2 and the CNTs results in efficient electrocatalytic performance for both OER and ORR [20]. The OER Tafel slope is 62 mV/dec at a potential of 0.78 V vs. Ag/AgCl. WS_2-CNT also delivers about a 4-electron transfer for ORR with a half-wave potential of −0.17 V vs. Ag/AgCl. This suggests that WS_2-CNT allow the ZAD to be charged at a much lower cell voltage, which results in lower energy consumption.

4. Conclusions

We introduce a new technology for high-performance electrochemical desalination using metal–air battery technology: zinc–air desalination (ZAD) using MoS_2 as a catalyst for OER and ORR at the cathode. Our system shows promising electrochemical performance, which translates into highly promising electrochemical desalination performance. The latter significantly exceeds that of present-day CDI or FDI. We see ZAD as a first contribution towards the establishment of metal–air desalination (MAD) technology.

CRediT authorship contribution statement

Pattarachai Srimuk: Conceptualization, Methodology, Writing - original draft, Visualization. **Lei Wang:** Data curation, Writing - review & editing. **Öznil Budak:** Data curation, Writing - review & editing, Visualization. **Volker Presser:** Conceptualization, Data curation, Writing - review & editing, Visualization.

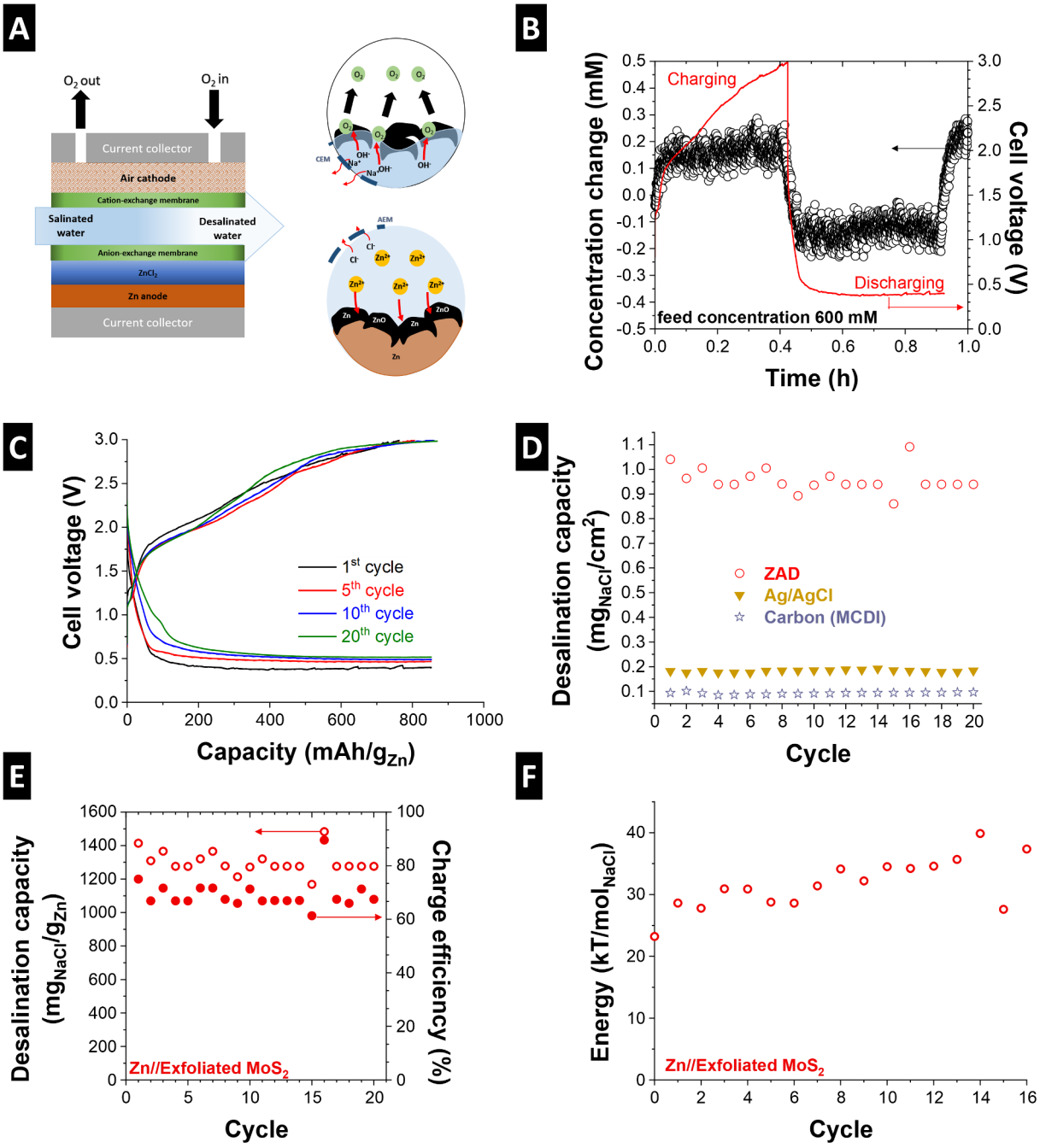

Fig. 4. Zinc–air desalination in 600 mM NaCl: (A) Illustration of ZAD cell configuration; (B) concentration change during charge and discharge of ZAD; (C) electrochemical performance (capacity vs. voltage profile); (D) area-normalized desalination capacity; (E) mass-normalized desalination capacity; (F) desalination-related energy consumption per mol of NaCl removed.

Table 1
Comparison of energy consumption using different electrode materials in solutions with a high salt concentration.

Electrode material (positive/negative)	Energy (kT or Wh/L)	References
$Mn_{0.44}MnO_2$/Ag	–/0.2	[7]
NaFeHCF/NaNiHCF	–/0.3	[21]
Carbon/V_2O_5	17.9/7.2	[22]
Carbon/TiS_2	30/1.2	[23]
AgCl/Ag	2.5/–	[12]
$ZnCl_2$/NaBr	–/8	[9]
MoS_2/Zn	92/0.008	This work

Declaration of Competing Interest

The authors declare that they have no known competing financial interests or personal relationships that could have appeared to influence the work reported in this paper.

Acknowledgments

We thank Eduard Arzt (INM) for his continuing support. L.W. acknowledges funding from the Chinese Scholarship Council (CSC) via award number 201906260277. V.P. and P.S. acknowledge support via

the electroMOXene project (PR-1173/9) by the German Research Foundation (DFG, Deutsche Forschungsgemeinschaft).

References

[1] N.M. Wade, Distillation plant development and cost update, Desalination 136 (2001) 3–12.

[2] F. Chen, Y. Huang, L. Guo, L. Sun, Y. Wang, H.Y. Yang, Dual-ions electrochemical deionization: a desalination generator, Energy Environ. Sci. 10 (2017) 2081–2089.

[3] M.E. Suss, S. Porada, X. Sun, P.M. Biesheuvel, J. Yoon, V. Presser, Water desalination via capacitive deionization: what is it and what can we expect from it? Energy Environ. Sci. 8 (2015) 2296–2319.

[4] S. Bi, Y. Zhang, L. Cervini, T. Mo, J.M. Griffin, V. Presser, G. Feng, Permselective ion electrosorption of subnanometer pores at high molar strength enables capacitive deionization of saline water, Sustain. Energy Fuels 4 (2020) 1285–1295.

[5] W. Bao, X. Tang, X. Guo, S. Choi, C. Wang, Y. Gogotsi, G. Wang, Porous cryo-dried MXene for efficient capacitive deionization, Joule 2 (2018) 778–787.

[6] K. Wang, Y. Liu, Z. Ding, Y. Li, T. Lu, L. Pan, Metal-organic frameworks derived $NaTi_2(PO_4)_3$/carbon composite for efficient hybrid capacitive deionization, J. Mater. Chem. A 7 (2019) 12126–12133.

[7] M. Pasta, C.D. Wessells, Y. Cui, F. La Mantia, A desalination battery, Nano Lett. 12 (2012) 839–843.

[8] P. Srimuk, F. Kaasik, B. Krüner, A. Tolosa, S. Fleischmann, N. Jäckel, M.C. Tekeli, M. Aslan, M.E. Suss, V. Presser, MXene as a novel intercalation-type pseudocapacitive cathode and anode for capacitive deionization, J. Mater. Chem. A 4 (2016) 18265–18271.

[9] S. Abu Khalla, M.E. Suss, Desalination via chemical energy: an electrodialysis cell driven by spontaneous electrode reactions, Desalination 467 (2019) 257–262.

[10] J. Lee, P. Srimuk, R.L. Zornitta, M. Aslan, B.L. Mehdi, V. Presser, High electrochemical seawater desalination performance enabled by an iodide redox electrolyte paired with a sodium superionic conductor, ACS Sustain. Chem. Eng. 7 (2019) 10132–10142.

[11] J. Ahn, J. Lee, S. Kim, C. Kim, J. Lee, P.M. Biesheuvel, J. Yoon, High performance electrochemical saline water desalination using silver and silver-chloride electrodes, Desalination 476 (2020) 114216.

[12] P. Srimuk, S. Husmann, V. Presser, Low voltage operation of a silver/silver chloride battery with high desalination capacity in seawater, RSC Adv. 9 (2019) 14849–14858.

[13] E. Davari, D.G. Ivey, Bifunctional electrocatalysts for Zn-air batteries, Sustain. Energy Fuels 2 (2018) 39–67.

[14] P. Srimuk, J. Lee, S. Fleischmann, S. Choudhury, N. Jäckel, M. Zeiger, C. Kim, M. Aslan, V. Presser, Faradaic deionization of brackish and sea water via pseudocapacitive cation and anion intercalation into few layered molybdenum disulfide, J. Mater. Chem. A 5 (2017) 15640–15649.

[15] P. Srimuk, L. Ries, M. Zeiger, S. Fleischmann, N. Jäckel, A. Tolosa, B. Krüner, M. Aslan, V. Presser, High performance stability of titania decorated carbon for desalination with capacitive deionization in oxygenated water, RSC Adv. 6 (2016) 106081–106089.

[16] Y. Li, H. Dai, Recent advances in zinc-air batteries, Chem. Soc. Rev. 43 (2014) 5257–5275.

[17] N. Kim, J. Lee, S. Kim, S.P. Hong, C. Lee, J. Yoon, C. Kim, Short review of multichannel membrane capacitive deionization: principle, current status, and future prospect, Appl. Sci. 10 (2020) 683.

[18] V. Pothanamkandathil, J. Fortunato, C.A. Gorski, Electrochemical desalination using intercalating electrode materials: a comparison of energy demands, Environ. Sci. Technol. (2020), https://doi.org/10.1021/acs.est.1029b07311.

[19] H.-F. Wang, C. Tang, Q. Zhang, A review of precious-metal-free bifunctional oxygen electrocatalysts: rational design and applications in Zn-air batteries, Adv. Funct. Mater. 28 (2018) 1803329.

[20] A.P. Tiwari, D. Kim, Y. Kim, H. Lee, Bifunctional oxygen electrocatalysis through chemical bonding of transition metal chalcogenides on conductive carbons, Adv. Energy Mater. 7 (2017) 1602217.

[21] J. Lee, S. Kim, J. Yoon, Rocking chair desalination battery based on Prussian Blue electrodes, ACS Omega 2 (2017) 1653–1659.

[22] J. Lee, P. Srimuk, K. Aristizabal, C. Kim, S. Choudhury, Y.-C. Nah, F. Mücklich, V. Presser, Pseudocapacitive desalination of brackish water and seawater with vanadium-pentoxide-decorated multiwalled carbon nanotubes, ChemSusChem 10 (2017) 3611–3623.

[23] P. Srimuk, J. Lee, A. Tolosa, C. Kim, M. Aslan, V. Presser, Titanium disulfide: a promising low-dimensional electrode material for sodium ion intercalation for seawater desalination, Chem. Mater. 29 (2017) 9964–9973.